Nanoscale

ROYAL SOCIETY OF CHEMISTRY

PAPER

View Article Online
View Journal | View Issue

Cite this: *Nanoscale*, 2022, **14**, 7674

Electrical control of biexciton Auger recombination in single CdSe/CdS nanocrystals†

Ying Tang,[a] Qilin Qin,[a] Hongyu Yang,[b] Shengnan Feng,[a] Chunfeng Zhang,[a] Jiayu Zhang, *[b] Min Xiao[a,c] and Xiaoyong Wang *[a]

Received 17th January 2022,
Accepted 7th May 2022

DOI: 10.1039/d2nr00305h

rsc.li/nanoscale

The Auger recombination effect is strongly enhanced in semiconductor nanocrystals due to the quantum confinement, and various strategies in chemical synthesis have been employed so far to suppress this nonradiative decay pathway of multiple excitons. Here we apply external electric fields on single CdSe/CdS giant nanocrystals at room temperature, showing that the biexciton Auger and single-exciton radiative rates can be averagely decreased by ~40 and ~10%, respectively. In addition to a reduced overlap of the electron–hole wavefunctions, the large decrease of biexciton Auger rate could be contributed by the enhanced exciton–exciton repulsion, while the electron–hole exchange interaction might be weakened to cause the relatively small decrease of the single-exciton radiative rate. The above findings have thus proved that the external electric field can serve as a post-synthetic knob to tune the exciton recombination dynamics in semiconductor nanocrystals towards their efficient applications in various optoelectronic devices.

Introduction

When a semiconductor is being optically or electrically excited, it is possible for the recombination energy of an exciton to be transferred to an extra charge instead of being converted to a photon.[1] It has been shown that this Auger recombination effect is greatly enhanced in the quantum-confined colloidal nanocrystals (NCs),[2] owing to the strong Coulomb interaction among charge carriers and the alleviated requirement for energy and momentum conservations.[3,4] Such nonradiative dissipation of multiple and charged excitons in the NC ensembles not only poses stringent limits on the optical-gain lifetime and wavelength bandwidth that can be achieved in the laser operations,[5,6] but also causes the efficiency roll-off issue in the light-emitting diodes.[7–9] Meanwhile, the Auger recombination of charged excitons would give rise to the photoluminescence (PL) blinking effect in a single colloidal NC,[10,11] with the intermittent appearance of non-emitting "off" periods being detrimental to the bio-related applications such as single-molecule imaging and labelling.[12,13]

Based on the fact that the rate of Auger recombination is inversely proportional to the spatial volume of charge confinement,[14,15] a practical way for its effective suppression has been realized in the CdSe/CdS giant NCs (*g*NCs) wherein the small CdSe core is surrounded by more than 10 monolayers of a large CdS shell.[16,17] It was also speculated that this suppression might be additionally contributed by the unintentional formation of a gradient alloy between the CdSe core and the CdS shell,[18,19] resulting in a smoothed interface potential to greatly reduce the overlap between the carrier initial and final states involved in the Auger recombination process.[20] This opinion was further corroborated by the controlled growth of an alloy layer to bridge the CdSe core and the CdS shell, which significantly boosted the emission efficiencies of both multiple and charged excitons as compared to those measured for an otherwise abrupt core–shell boundary.[21,22]

It should be equally noted that, in a single CdSe/CdS *g*NC, the electron wavefunction is spatially delocalized into the CdS shell while the hole wavefunction is tightly confined inside the CdSe core.[19,22] As a result of the quasi-type-II energy-level alignment, the electron–hole Coulomb interaction is strongly reduced to mitigate the Auger recombination effect, as was similarly observed in the colloidal CdTe/CdSe core–shell[23,24] and CdSe/CdS dot-in-rod[25] nanostructures. In contrast to the volume or alloy control that irreversibly yields one batch of CdSe/CdS *g*NCs with fixed photophysical properties, the spatial separation of electron–hole wavefunctions can potentially serve as a post-synthetic knob to tune the degree of Auger recombination by means of an external stimulus such as

[a]*National Laboratory of Solid State Microstructures, School of Physics, and Collaborative Innovation Center of Advanced Microstructures, Nanjing University, Nanjing 210093, China. E-mail: wxiaoyong@nju.edu.cn*
[b]*Advanced Photonics Center, School of Electronic Science and Engineering, Southeast University, Nanjing 210096, China. E-mail: jyzhang@seu.edu.cn*
[c]*Department of Physics, University of Arkansas, Fayetteville, Arkansas 72701, USA*
†Electronic supplementary information (ESI) available. See DOI: **https://doi.org/10.1039/d2nr00305h**

the electric field. So far, the quantum-confined Stark effect (QCSE) has been studied at the single-exciton regime in colloidal NCs with various compositions and shapes,[26–30] however, the powerfulness of an external electric field in modifying the multi-exciton recombination dynamics is still largely unexplored.

In this report, we perform electro-optical studies on single CdSe/CdS *g*NCs at room temperature, showing that the exciton recombination dynamics are more sensitive to the external electric field than the PL spectral responses. For most of the studied single CdSe/CdS *g*NCs, the single-exciton radiative and biexciton Auger rates decrease or increase synchronously with the variation of an external electric field, signifying the reduced or enlarged overlap of the electron–hole wavefunctions. The reduced wavefunction overlap in a single CdSe/CdS *g*NC is accompanied by the enhancement of the exciton–exciton repulsive interaction, leading to a larger percentage decrease of the biexciton Auger rate than that of the single-exciton radiative rate. Meanwhile, the enlarged wavefunction overlap is caused by the cancelling of an internal electric field related to the permanent dipole moment, whose existence can be deduced from the blue-shifted PL peak observed in a single CdSe/CdS *g*NC under the external electric field. In some other single CdSe/CdS *g*NCs, it is interesting to see that the single-exciton radiative rate is always increased upon the application of a positive or negative external electric field, although the associated decrease of the biexciton Auger rate does suggest a reduced overlap of the electron–hole wavefunctions. This abnormal behavior is explained by the electric-field induced weakening of the electron–hole exchange interaction, which can promote thermal activation of more single excitons from the dark to the bright states due to their reduced energy separation.

Experimental

Chemical synthesis of CdSe/CdS *g*NCs

Following the standard procedures as reported previously,[31,32] the CdSe/CdS *g*NCs used in the current experiment are synthesized with a core diameter of ~4.0 nm and a shell thickness of ~11 monolayers. The average size of the as-synthesized CdSe/CdS *g*NCs is estimated to be ~10.8 nm according to the transmission electron microscopy (TEM) measurements (Fig. S1†), with the band-edge absorption and emission peaks being located at ~633 and ~645 nm, respectively (Fig. S2†).

Optical measurements

For the optical measurements at room temperature, one drop of the diluted solution is spin-coated onto a SiO_2 substrate to place single CdSe/CdS *g*NCs between two electrodes each with a width of 10 μm and separated by 5 μm in an interdigitated pattern (Fig. S3†). The sample substrate is positioned in a home-built confocal scanning optical microscope, where each single CdSe/CdS *g*NC is excited at 405 nm by a 5 MHz picosecond laser. The PL signal of a single CdSe/CdS *g*NC can be sent to either a charge-coupled-device (CCD) camera for the PL spectral measurement with an integration time of 1 s, or two avalanche photodiodes (APDs) for the PL decay and the second-order photon correlation $g^{(2)}(\tau)$ measurements with a time resolution of ~100 ps.

Results and discussion

In Fig. 1a, we plot the PL spectrum measured for a representative single CdSe/CdS *g*NC with a peak wavelength of ~650 nm and a linewidth of ~20 nm. The PL intensities of this single CdSe/CdS *g*NC excited at increasing laser power densities are plotted in Fig. 1b, which can be fitted with a functional form, $\propto 1 - e^{-\alpha P} = 1 - e^{-\langle N\rangle}$. Here, α is a fitting constant related to the absorption cross section, P is the laser power density, and $\langle N\rangle$ is the average number of excitons created per pulse in a single CdSe/CdS NC.[4,33] In the following optical studies of single CdSe/CdS *g*NCs, the laser power density is specifically chosen to set $\langle N\rangle$ at either ~0.1 or ~0.5, corresponding to the dominant presence of single excitons or the additional generation of biexcitons, respectively. The $g^{(2)}(\tau)$ curves measured at $\langle N\rangle$ = ~0.1 for three representative single CdSe/CdS *g*NCs are plotted in Fig. S4,† confirming that a single quantum emitter is being studied in our experiment.[34]

The PL intensity time trace measured for a single CdSe/CdS *g*NC at $\langle N\rangle$ = ~0.1 is plotted in Fig. 1c, where the blinking

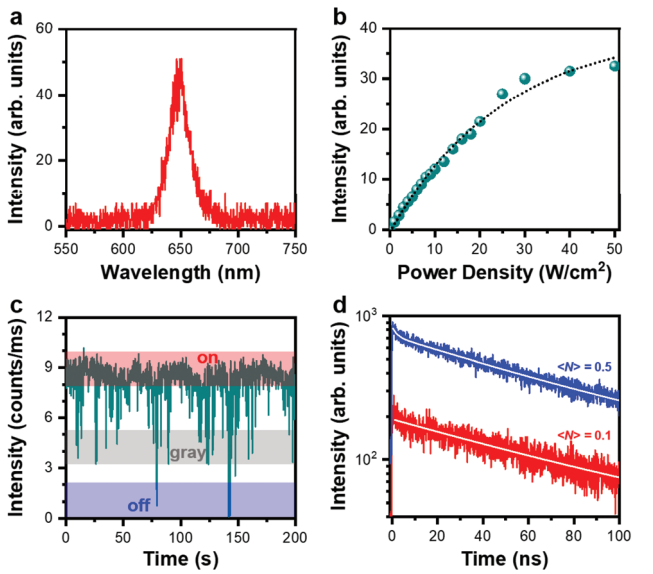

Fig. 1 Fundamental optical properties of single CdSe/CdS *g*NCs. (a) PL spectrum measured for a single CdSe/CdS *g*NC. (b) PL intensity measured for this single CdSe/CdS *g*NC as a function of the laser power density. The data points are fitted by the dotted line using the functional form, $\propto 1 - e^{-\alpha P}$, with α and P being a fitting constant (~3.9 × 10^{-2} cm^2 W^{-1}) and the laser power density, respectively. (c) PL intensity time trace measured at $\langle N\rangle$ = ~0.1 for a single CdSe/CdS *g*NC with a binning time of 10 ms. The "on", "gray" and "off" states are marked by the red, gray and blue shadings, respectively. (d) PL decay curves measured at $\langle N\rangle$ = ~0.1 and ~0.5 for the "on" state of this single CdSe/CdS *g*NC, and fitted by the single- and bi-exponential functions, respectively.

"on", "gray" and "off" periods should arise from the neutral, negatively-charged and positively-charged single excitons, respectively.[35] As shown in Fig. 1d for the $\langle N\rangle$ = ~0.1 case, the PL decay curve extracted from the "on" state photons of this single CdSe/CdS *g*NC can be fitted by a single-exponential function, with a lifetime of ~87.6 ns for the radiative recombination of neutral single excitons ($\tau_{X,\ rad}$). For the same single CdSe/CdS *g*NC but excited at $\langle N\rangle$ = ~0.5, the "on" state PL decay curve also plotted in Fig. 1d can only be fitted well by a bi-exponential function. In addition to the slow lifetime already extracted above at $\langle N\rangle$ = ~0.1, the short lifetime of ~2.1 ns ($\tau_{XX,\ total}$) should be jointly contributed by the radiative ($\tau_{XX,\ rad}$) and Auger ($\tau_{XX,\ Auger}$) recombination processes of neutral biexcitons. Using $\tau_{X,\ rad} = 4\tau_{XX,\ rad}$ and $1/\tau_{XX,\ total} = 1/\tau_{XX,\ rad} + 1/\tau_{XX,\ Auger}$,[35] we can estimate the biexciton Auger lifetime of $\tau_{XX,\ Auger}$ to be ~2.3 ns for this specific single CdSe/CdS *g*NC. From the PL decay measurements of ~50 single CdSe/CdS *g*NCs at $\langle N\rangle$ = ~0.5, the obtained $\tau_{X,\ rad}$ and $\tau_{XX,\ Auger}$ values are statistically averaged at 56.2 ± 14.1 and 5.0 ± 4.5 ns, respectively (Fig. S5†). The $\tau_{XX,\ Auger}$ values here are several times longer than those obtained previously for single CdSe/CdS *g*NCs with similar sizes,[36] implying an effective suppression of the Auger recombination effect, which can also be deduced from the relatively long PL lifetimes measured for the blinking "gray" and "off" periods (see Fig. S6† for one example).

After the above fundamental characterizations of single CdSe/CdS *g*NCs, we move to the next step to explore how their optical properties are influenced by the external electric field. In Fig. 2a, we demonstrate a confocal scanning optical image containing the PL spots from several single CdSe/CdS *g*NCs located between two nearby electrodes. When excited at $\langle N\rangle$ = ~0.5 and biased under the electric field up to ±400 kV cm^{-1}, 53 out of the 100 studied single CdSe/CdS *g*NCs show undetectable optical responses in terms of the PL peak shift and the PL lifetime change. On the other hand, the rest 47 single CdSe/CdS *g*NCs can be further classified into four types according to their different optical responses to the external electric field (see the following descriptions and Table S1†).

For the first type of five single CdSe/CdS *g*NCs biased under a positive or negative electric field, a red shift of the PL peak can be observed due to an increased separation between the electron–hole wavefunctions. This nearly symmetric shift about the zero field, which represents a normal QCSE in semiconductor nanostructures,[37,38] is representatively shown in Fig. 2b for a single CdSe/CdS *g*NC (see Fig. S7a† for one more example). Upon the application of a positive (negative) electric field of 400 (−400) kV cm^{-1}, the PL peak changes from ~1.9159 to ~1.9042 (~1.8974) eV, corresponding to a reduction of the bandgap energy by ~11.7 (~18.5) meV. For the second type of four single CdSe/CdS *g*NCs, the PL peak shows an obvious asymmetric shift about the zero field, and this abnormal QCSE can be attributed to the existence of an internal electric field related to the permanent dipole moment.[30] As shown in Fig. 2c for such a single CdSe/CdS *g*NC (see Fig. S7b† for one more example), the internal electric field has already

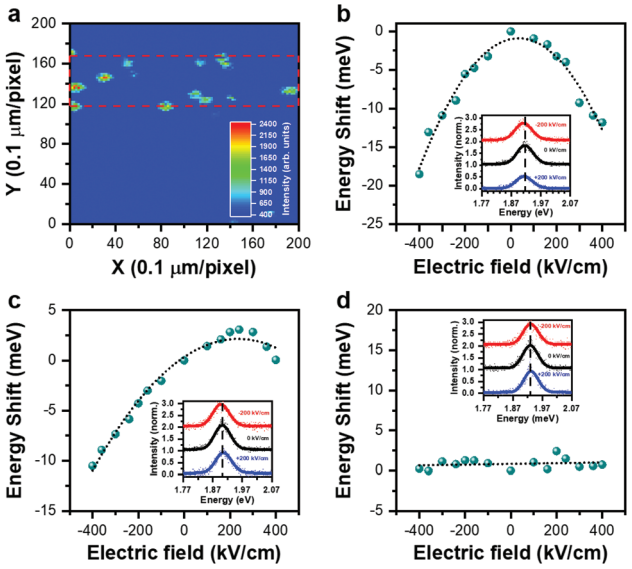

Fig. 2 Electric-field influence on the PL spectrum. (a) Confocal scanning optical image of the sample substrate showing the PL spots from several single CdSe/CdS *g*NCs. The red dashed box marks the spatial region between two nearby electrodes. PL peak energy shift measured as a function of the external electric field for a single CdSe/CdS *g*NC belonging to the (b) first, (c) second or (d) third type, respectively, with the black dotted line being plotted for the eye-guiding purpose. In the inset of (b), (c) or (d), three representative PL spectra measured at the electric fields of −200, 0 and 200 kV cm^{-1} are plotted for the single CdSe/CdS *g*NC, while the black dashed line marks the peak position of the zero-field PL spectrum. In (b) and (c), the degree of PL peak energy shift is reproducible whenever the same electric field is applied, thus excluding its possible origin from the spectral diffusion effect.

caused a red shift in the PL peak, which is shifted further from ~1.9033 to ~1.8926 eV when the external electric field is decreased from 0 to −400 kV cm^{-1}, corresponding to a reduction of the bandgap energy by ~10.7 meV. With the increase of the external electric field from 0 to 200 kV cm^{-1}, the internal electric field is gradually cancelled to cause a blue shift of the PL peak from ~1.9033 to ~1.9059 eV, corresponding to an increase of the bandgap energy by ~2.6 meV. After the internal electric field is completely removed, a further increase of the external electric field shifts the PL peak again to the red side until it gets to the energy position of ~1.9030 eV at 400 kV cm^{-1}. As proposed previously in several reports,[39,40] the lattice mismatch and the accompanied strain in the core/shell interface could give rise to the permanent dipole moment observed here in a single CdSe/CdS *g*NC by means of the piezoelectric effect. In contrast, the third type of 30 and the fourth type of eight single CdSe/CdS *g*NCs demonstrate no obvious shift in the PL peak under the external electric field (see Fig. 2d and Fig. S7c† for two examples), however, significant changes in their PL lifetimes can still be probed as will be discussed later in the text.

In Fig. 3, we plot the PL decay curves measured at $\langle N\rangle$ = ~0.5 for one representative single CdSe/CdS *g*NC from each of the four types, whose $\tau_{X,\ rad}$, $\tau_{XX,\ total}$ and $\tau_{XX,\ Auger}$ values

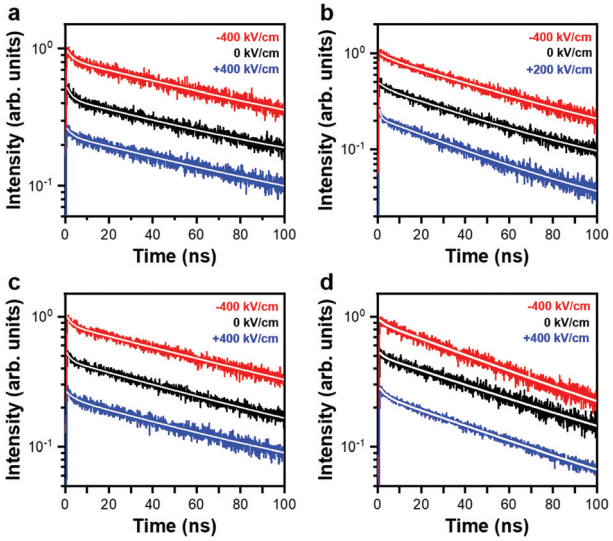

Fig. 3 Electric-field influence on the PL lifetime. (a) PL decay curves measured for a single CdSe/CdS *g*NC from the first type at the electric fields of −400, 0 and 400 kV cm^{-1}, respectively. (b) PL decay curves measured for a single CdSe/CdS *g*NC from the second type at the electric fields of −400, 0 and 200 kV cm^{-1}, respectively. (c) PL decay curves measured for a single CdSe/CdS *g*NC from the third type at the electric fields of −400, 0 and 400 kV cm^{-1}, respectively. (d) PL decay curves measured for a single CdSe/CdS *g*NC from the fourth type at the electric fields of −400, 0 and 400 kV cm^{-1}, respectively. In (a)–(d), the three PL decay curves are offset to each other for clarity, and each PL decay curve is fitted by the solid line using a bi-exponential function (see Table 1 for the fitted lifetime values).

obtained at different electric fields are listed in Table 1 (see Fig. S8† for these PL decay curves plotted at longer acquisition times). For the first type of five single CdSe/CdS *g*NCs with the normal QCSE, $\tau_{X,\ rad}$, $\tau_{XX,\ total}$ and $\tau_{XX,\ Auger}$ would increase with the increasing amplitude of the positive or negative electric field (Fig. 3a and Table 1). From the second type of four single CdSe/CdS *g*NCs with the abnormal QCSE, we similarly observe that a red shift in the PL peak is accompanied by the simultaneous increases of $\tau_{X,\ rad}$, $\tau_{XX,\ total}$ and $\tau_{XX,\ Auger}$ (Fig. 3b and Table 1). On the other hand, $\tau_{X,\ rad}$, $\tau_{XX,\ total}$ and $\tau_{XX,\ Auger}$ would decrease when the PL peak is shifted to the blue side (Fig. 3b and Table 1), signifying again that the external electric field could enlarge the overlap of the electron–hole wavefunctions by cancelling out the internal electric field. For the third type of 30 single CdSe/CdS *g*NCs showing no obvious PL peak shift, the $\tau_{X,\ rad}$, $\tau_{XX,\ total}$ and $\tau_{XX,\ Auger}$ values can still be significantly increased whenever a positive or negative electric field is applied (Fig. 3c and Table 1). From the fourth type of eight single CdSe/CdS *g*NCs also showing no obvious PL peak shift, it is interesting to see that the positive or negative electric field can still induce the increases of $\tau_{XX,\ total}$ and $\tau_{XX,\ Auger}$ but an unexpected decrease of $\tau_{X,\ rad}$ (Fig. 3d and Table 1).

In Fig. S9,† we provide the PL decay curves measured at $\langle N \rangle$ = ~0.5 for one more single CdSe/CdS *g*NC from each of the four types, showing that it is quite common for the single-exciton and biexciton lifetimes to be modulated by an external electric field. Compared to the single CdSe/CdS *g*NCs in the first two types, the ones in the third and fourth types might be associated with a stronger quantum-confinement effect, so that it is not easy for the external electric field to modulate the electron–hole wavefunctions enough for a detectable change of the emission wavelength. However, this modulation is already sufficient to change the exciton recombination dynamics in a single CdSe/CdS *g*NC, suggesting that the QCSE of semiconductor nanostructures, normally defined within the context of emission wavelength, should be extended to the regime of PL lifetime that is more sensitive to the perturbance of an external electric field.

Using $k_{X,\ rad} = 1/\tau_{X,\ rad}$ and $k_{XX,\ Auger} = 1/\tau_{XX,\ Auger}$ for the single-exciton radiative and biexciton Auger rates, respectively, we demonstrate in Fig. 4a how they are changed by the same electric fields applied to a representative single CdSe/CdS *g*NC from the third type. The measured $k_{X,\ rad}$ value is ~0.020 ns^{-1} at 0 kV cm^{-1}, and it decreases to ~0.017 and ~0.016 ns^{-1} at

Table 1 PL lifetimes obtained at various electric fields for four single CdSe/CdS *g*NCs excited at $\langle N \rangle$ = ~0.5. The PL decay curves shown in Fig. 3 are each fitted by the bi-exponential function of $A_1 \exp(-t/\tau_{XX,\ total}) + A_2 \exp(-t/\tau_{X,\ rad})$. $\tau_{XX,\ total}$, $\tau_{X,\ rad}$ and $\tau_{XX,\ Auger}$ denote the biexciton PL lifetime, single-exciton radiative lifetime and biexciton Auger lifetime, respectively

Types/figures	Electric field (kV cm^{-1})	A_1	$\tau_{XX,\ total}$ (ns)	A_2	$\tau_{X,\ rad}$ (ns)	$\tau_{XX,\ Auger}$ (ns)	Adjusted *R*-square
Type 1/Fig. 3a	−400	0.04	2.9 ± 0.1	0.84	96.6 ± 2.3	3.3 ± 0.1	0.96
	0	0.05	2.2 ± 0.2	0.58	84.4 ± 1.7	2.5 ± 0.3	0.96
	400	0.02	2.7 ± 0.2	0.75	96.0 ± 2.2	3.0 ± 0.2	0.96
Type 2/Fig. 3b	−400	0.03	4.9 ± 0.1	0.89	57.6 ± 1.6	7.4 ± 0.1	0.95
	0	0.02	2.8 ± 0.1	0.70	49.5 ± 0.8	3.7 ± 0.2	0.96
	200	0.08	0.8 ± 0.1	0.80	43.4 ± 0.5	0.9 ± 0.1	0.96
Type 3/Fig. 3c	−400	0.01	2.5 ± 0.2	0.83	94.5 ± 3.1	2.8 ± 0.2	0.97
	0	0.02	2.0 ± 0.2	0.79	83.6 ± 1.5	2.2 ± 0.2	0.98
	400	0.01	3.5 ± 0.4	0.77	85.4 ± 2.4	4.2 ± 0.6	0.96
Type 4/Fig. 3d	−400	0.009	2.6 ± 0.2	0.23	67.2 ± 1.6	3.1 ± 0.2	0.99
	0	0.003	2.0 ± 0.2	0.43	73.7 ± 1.5	2.3 ± 0.2	0.97
	400	0.004	3.0 ± 0.1	0.78	69.9 ± 1.1	3.6 ± 0.2	0.98

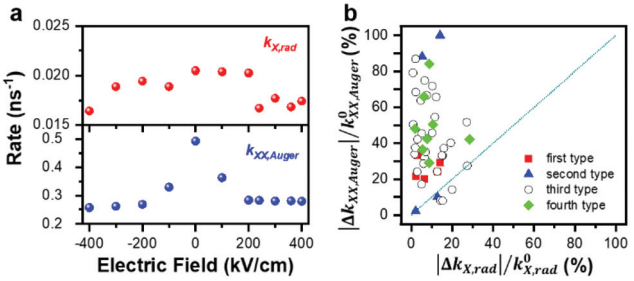

Fig. 4 Percentage changes of the single-exciton radiative and biexciton Auger rates. (a) Single-exciton radiative rate ($k_{X,\ rad}$) and biexciton Auger rate ($k_{XX,\ Auger}$) plotted as a function of the external electric field for a single CdSe/CdS *g*NC from the third type. (b) Correlated data point plotted for the percentage changes of the biexciton Auger rate ($|\Delta k_{XX,\ Auger}|/k^0_{XX,Auger}$) and the single-exciton radiative rate ($|\Delta k_{X,\ rad}|/k^0_{X,rad}$) obtained from each of the 47 single CdSe/CdS *g*NCs studied in the experiment. (■) The first type of five single CdSe/CdS *g*NCs. (▲) The second type of four single CdSe/CdS *g*NCs. (○) The third type of 30 single CdSe/CdS *g*NCs. (◆) The fourth type of eight single CdSe/CdS *g*NCs.

400 and −400 kV cm^{-1}, respectively. Meanwhile, the obtained $k_{XX,\ Auger}$ value is ~0.493 ns^{-1} at 0 kV cm^{-1}, and it decreases to ~0.279 and ~0.257 ns^{-1} at 400 and −400 kV cm^{-1}, respectively. As similarly observed in other single CdSe/CdS *g*NCs, the maximum changes of $k_{X,\ rad}$ and $k_{XX,\ Auger}$ from their zero-field values, denoted by $\Delta k_{X,\ rad}$ and $\Delta k_{XX,\ Auger}$, always occur simultaneously at a specific electric-field value within the range from −400 to 400 kV cm^{-1}.

We can then define the percentage change of $k_{X,\ rad}$ ($k_{XX,\ Auger}$) as $|\Delta k_{X,\ rad}|/k^0_{X,rad}$ ($|\Delta k_{XX,\ Auger}|/k^0_{XX,Auger}$), where $k^0_{X,rad}$ ($k^0_{XX,Auger}$) is the zero-field value and the absolute value sign is used since $\Delta k_{X,\ rad}$ ($\Delta k_{XX,\ Auger}$) could be a negative value. Specifically, $\Delta k_{X,\ rad}$ and $\Delta k_{XX,\ Auger}$ are both negative for the first and third types of single CdSe/CdS *g*NCs, and they are both positive for the second type of single CdSe/CdS NCs. In this sense, the first three types of single CdSe/CdS *g*NCs can be jointly discussed owing to the same increasing or decreasing trend of $k_{X,\ rad}$ and $k_{XX,\ Auger}$ with the variation of the external electric field. For the single CdSe/CdS *g*NC studied in Fig. 4a, the percentage changes of $k_{X,\ rad}$ and $k_{XX,\ Auger}$ are estimated to be ~20.0 and ~47.9%, respectively, whose correlated point is plotted in Fig. 4b together with those obtained for all the other single CdSe/CdS *g*NCs from the first three types.

It can be seen from Fig. 4b that except several data points, all the other ones are distributed above the diagonal line with the percentage changes of $k_{X,\ rad}$ and $k_{XX,\ Auger}$ being averaged at ~9.3 ± 7.0 and ~41.8 ± 24.5%, respectively. This suggests that the biexciton Auger recombination in a single CdSe/CdS *g*NC is more influenced by the external electric field than the single-exciton radiative recombination. Due to the quasi-type-II energy-level alignment with a broken local-charge neutrality, there should exist a repulsive interaction between the single exciton and biexciton in a single CdSe/CdS *g*NC.[41] This exciton–exciton repulsion effect was previously confirmed from the optical studies of single CdSe/CdS *g*NCs at cryogenic temperature, showing that the PL peak of biexciton was blue-shifted relative to that of the single exciton.[42] When a single CdSe/CdS *g*NC is biased by the external electric field, the two electrons (holes) would be forced to occupy the same shell (core) region with their mutual repulsion being reinforced to decelerate the biexciton Auger recombination process.[18,23] Consequently, the reduced overlap of electron–hole wavefunctions by the external electric field leads to an average percentage change of ~9.3% in $k_{X,\ rad}$ at the first place, and it further cooperates with the reinforced exciton–exciton repulsion to yield a percentage change of $k_{XX,\ Auger}$ that is averaged at a larger value of ~41.8%.

From the fourth type of eight single CdSe/CdS NCs, we observe a positive $\Delta k_{X,\ rad}$ and a negative $\Delta k_{XX,\ Auger}$ upon the application of an external electric field, which are at odds with their synchronous changes possessed by the first three types. For comparison, the percentage changes of $k_{X,\ rad}$ and $k_{XX,\ Auger}$ for these eight single CdSe/CdS *g*NCs are also plotted in Fig. 4b with the average values of ~9.7 ± 8.0 and ~49.9 ± 17.6%, respectively. While the decrease of $k_{X,\ Auger}$ can still be explained by the joint effect of the reduced overlap of electron–hole wavefunctions and the reinforced exciton–exciton repulsion, some other mechanisms have to be invoked to accommodate the increase of $k_{X,\ rad}$ under both the positive and negative electric fields. In semiconductor colloidal NCs, the trap-state emission is normally manifested as a red-shifted PL peak relative to that of the quantum-confined state emission,[43] which are not observed in our single CdSe/CdS *g*NCs (see Fig. 1a and Fig. S2†). Meanwhile, the trap states should be associated with a longer PL lifetime than that of the quantum-confined state,[43] which is also against the fact that we always observe a single-exponential PL lifetime when a single CdSe/CdS *g*NC is excited at a low laser power density (see Fig. 1d). Most importantly, the trap states should bear the bulk semiconductor feature with a continuous distribution, so that the electrical modulation of their optical properties are not expected. Based on the above discussions, we tend to exclude the existence of trap states in a single CdSe/CdS *g*NC as a possible origin for its increased $k_{X,\ rad}$ under the external electric field.

For standard core-only CdSe NCs, the two lowest band-edge states are occupied by the higher-energy bright and lower-energy dark excitons, respectively, whose separation is positively correlated with the electron–hole exchange interaction.[44] On the other hand, this electron–hole exchange interaction is linearly proportional to the overlap of the electron–hole wavefunctions, which would be decreased in the CdSe/CdS *g*NCs with an increasing shell thickness.[45] As revealed from the effective mass calculations,[45] the energy separation of the bright and dark states in the CdSe/CdS *g*NCs ranges from hundreds of μeV to several meV, which is significantly smaller than the thermal energy of ~24 meV at room temperature. As a consequence, the single-exciton radiative rate measured here for single CdSe/CdS *g*NCs should be strongly dependent on the degree of thermal mixing between the bright and dark states.[46] When an external electric field is applied to a single CdSe/CdS *g*NC to reduce the overlap of the electron–hole wave-

functions, the energy separation of the bright and dark states would be deceased due to the weakened electron–hole exchange interaction. The thermal occupancy probability of single excitons in the bright state would be thus increased, resulting in an overall acceleration of the radiative recombination rate.[46–48] While the above scenario is applicable to the fourth type of single CdSe/CdS *g*NCs, it is possible that the energy separation of bright and dark states in the first three types is either too large or too small, so that their relative thermal occupancies could not be effectively tuned by the external electric field. In these two cases under an external electric field, the increased single-exciton radiative lifetime caused by the reduced overlap of electron–hole wavefunctions would be dominant over the decreased single-exciton radiative lifetime caused by the weakened electron–hole exchange interaction.

In our experiment, two specific laser power densities are employed to set either $\langle N \rangle$ = ~0.1 or ~0.5 for a single CdSe/CdS *g*NC, according to the average absorption cross section estimated from the PL intensity saturation measurement (see Fig. 1b). In this case, mainly single excitons are created at $\langle N \rangle$ = ~0.1 while both single excitons and biexcitons are present at $\langle N \rangle$ = ~0.5 inside a single CdSe/CdS *g*NC,[49,50] so that we can apply the statistical scaling law dictating a ratio of four between their radiative lifetimes without the influence of higher-order excitons (see Fig. S10† for the PL decay curves measured at different exciton numbers). However, there should exist a variation of this ratio among the studied single CdSe/CdS *g*NCs, especially under the influence of the exciton–exciton repulsion effect,[36] which might cause an uncertainty in estimating the biexciton Auger lifetime. Moreover, the relative contribution of biexcitons to the PL decay curve measured at $\langle N \rangle$ = ~0.5 for a single CdSe/CdS *g*NC is significantly smaller than that of the single excitons (see Table 1), which would cause a fitting uncertainty in determining the biexciton Auger lifetime. These two uncertainties could be minimized in future works by adopting single CdSe/CdS *g*NCs with high biexciton fluorescent efficiencies, isolating out the biexciton photons for a more precise estimation of the PL lifetime,[22] and obtaining the ratio between single-exciton and biexciton radiative lifetimes alternatively from the second-order photon correlation measurement.[22,36,51] It should be further noted that, besides the PL spectra and PL decay curves, the PL intensity time traces of some single CdSe/CdS *g*NCs can also be altered by the external electric field to yield a reduced occurrence of mainly the "gray" periods (see Fig. S11† for one example). Since no extra charge would be injected into or extracted from a single CdSe/CdS *g*NC by the external electric field, the above observation could also be explained by the suppressed Auger recombination of biexcitons with a reduced probability of photo-ionization.[4]

Conclusions

To summarize, we have applied the external electric field to single CdSe/CdS *g*NCs at room temperature, revealing that the QCSE is more manifested by the change of PL lifetime than the shift of PL spectrum. For most of the studied single CdSe/CdS *g*NCs with obvious electro-optical responses, the overlap of the electron–hole wavefunctions can be successfully reduced to yield the average percentage decreases of ~40 and ~10% in the biexciton Auger and single-exciton radiative rates, respectively. The relatively large decease of the biexciton Auger rate might be additionally contributed by the reinforced exciton–exciton repulsion, while the small change of the single-exciton radiative rate suggests that the electron–hole exchange interaction might be weakened to partially counteract the effectiveness of the reduced overlap between the electron–hole wavefunctions. This weakened electron–hole exchange interaction is further confirmed in some other single CdSe/CdS *g*NCs, whose electric-field induced decrease of the energy-level splitting would promote thermal activation of more single excitons from the dark to the bright states with an accelerated radiative rate. Although the ability for an external electric field to control the exciton–exciton repulsive interaction and the electron–hole exchange interaction is demonstrated here in single CdSe/CdS *g*NCs with a quasi-type-II energy-level alignment, it can also be extended to other semiconductor NCs with varying degrees of intrinsic overlap of the electron–hole wavefunctions. As such, our experimental results have provided a deeper understanding on the fundamental electro-optical properties of semiconductor NCs, which will surely guide their efficient usage in a variety of optoelectronic devices especially by taking advantage of the reduced biexciton Auger rate. For example, the charge carriers can still be efficiently collected when a solar-cell device is under intensive light illumination or subject to the carrier multiplication effect, and an intentional biasing with the external electric field should be helpful in circumventing the efficiency roll-off issue of the light-emitting diodes.

Author contributions

YT performed the optical measurements with the help of QQ and SF. HY synthesized the samples with the help of JZ. XW wrote the manuscript with the help of CZ and MX.

Conflicts of interest

There are no conflicts to declare.

Acknowledgements

This work is supported by the National Key Research and Development Program of China (no. 2019YFA0308700 and 2017YFA0303700), the National Natural Science Foundation of China (no. 62174081 and 61974058), and the Priority Academic Program Development of Jiangsu Higher Education Institutions.

References

1 P. T. Landsberg, *Recombination in Semiconductors*, Cambridge University Press, 2003.
2 D. I. Chepic, Al. L. Efros, A. I. Ekimov, M. G. Ivanov, V. A. Kharchenko, I. A. Kudriavtsev and T. V. Yazeva, *J. Lumin.*, 1990, **47**, 113–127.
3 V. I. Klimov, A. A. Mikhailovsky, D. W. McBranch, C. A. Leatherdale and M. G. Bawendi, *Science*, 2000, **287**, 1011–1013.
4 F. Hu, B. Lv, C. Yin, C. Zhang, X. Wang, B. Lounis and M. Xiao, *Phys. Rev. Lett.*, 2016, **116**, 106404.
5 V. I. Klimov, A. A. Mikhailovsky, S. Xu, A. Malko, J. A. Hollingsworth, C. A. Leatherdale, H.-J. Eisler and M. G. Bawendi, *Science*, 2000, **290**, 314–317.
6 F. Fan, O. Voznyy, R. P. Sabatini, K. T. Bicanic, M. M. Adachi, J. R. McBride, K. R. Reid, Y. S. Park, X. Li, A. Jain, R. Quintero-Bermudez, M. Saravanapavanantham, M. Liu, M. Korkusinski, P. Hawrylak, V. I. Klimov, S. J. Rosenthal, S. Hoogland and E. H. Sargent, *Nature*, 2017, **544**, 75–79.
7 Y. Shirasaki, G. J. Supran, W. A. Tisdale and V. Bulović, *Phys. Rev. Lett.*, 2013, **110**, 217403.
8 J. Lim, Y.-S. Park, K. Wu, H. J. Yun and V. I. Klimov, *Nano Lett.*, 2018, **18**, 6645–6653.
9 W. K. Bae, Y.-S. Park, J. Lim, D. Lee, L. A. Padilha, H. McDaniel, I. Robel, C. Lee, J. M. Pietryga and V. I. Klimov, *Nat. Commun.*, 2013, **4**, 2661.
10 M. Nirmal, B. O. Dabbousi, M. G. Bawendi, J. J. Macklin, J. K. Trautman, T. D. Harris and L. E. Brus, *Nature*, 1996, **383**, 802–804.
11 C. Galland, Y. Ghosh, A. Steinbrück, M. Sykora, J. A. Hollingsworth, V. I. Klimov and H. Htoon, *Nature*, 2011, **479**, 203–207.
12 I. L. Medintz, H. T. Uyeda, E. R. Goldman and H. Mattoussi, *Nat. Mater.*, 2005, **4**, 435–446.
13 F. Pinaud, S. Clarke, A. Sittner and M. Dahan, *Nat. Methods*, 2010, **7**, 275–285.
14 M. C. Beard, K. P. Knutsen, P. Yu, J. M. Luther, Q. Song, W. K. Metzger, R. J. Ellingson and A. J. Nozik, *Nano Lett.*, 2007, **7**, 2506–2512.
15 I. Robel, R. Gresback, U. Kortshagen, R. D. Schaller and V. I. Klimov, *Phys. Rev. Lett.*, 2009, **102**, 177404.
16 Y. Chen, J. Vela, H. Htoon, J. L. Casson, D. J. Werder, D. A. Bussian, V. I. Klimov and J. A. Hollingsworth, *J. Am. Chem. Soc.*, 2008, **130**, 5026–5027.
17 B. Mahler, P. Spinicelli, S. Buil, X. Quelin, J.-P. Hermier and B. Dubertret, *Nat. Mater.*, 2008, **7**, 659–664.
18 F. García-Santamaría, Y. Chen, J. Vela, R. D. Schaller, J. A. Hollingsworth and V. I. Klimov, *Nano Lett.*, 2009, **9**, 3482–3488.
19 C. Javaux, B. Mahler, B. Dubertret, A. Shabaev, A. V. Rodina, Al. L. Efros, D. R. Yakovlev, F. Liu, M. Bayer, G. Camps, L. Biadala, S. Buil, X. Quelin and J.-P. Hermier, *Nat. Nanotechnol.*, 2013, **8**, 206–212.
20 G. E. Cragg and A. L. Efros, *Nano Lett.*, 2010, **10**, 313–317.
21 W. K. Bae, L. A. Padilha, Y.-S. Park, H. McDaniel, I. Robel, J. M. Pietryga and V. I. Klimov, *ACS Nano*, 2013, **7**, 3411–3419.
22 Y.-S. Park, W. K. Bae, L. A. Padilha, J. M. Pietryga and V. I. Klimov, *Nano Lett.*, 2014, **14**, 396–402.
23 D. Oron, M. Kazes and U. Banin, *Phys. Rev. B: Condens. Matter Mater. Phys*, 2007, **75**, 035330.
24 R. Osovsky, D. Cheskis, V. Kloper, A. Sashchiuk, M. Kroner and E. Lifshitz, *Phys. Rev. Lett.*, 2009, **102**, 197401.
25 M. Zavelani-Rossi, M. G. Lupo, F. Tassone, L. Manna and G. Lanzani, *Nano Lett.*, 2010, **10**, 3142–3150.
26 S. A. Empedocles and M. G. Bawendi, *Science*, 1997, **278**, 2114–2117.
27 F. Vietmeyer, T. Tchelidze, V. Tsou, B. Janko and M. Kuno, *ACS Nano*, 2012, **6**, 9133–9140.
28 E. Rothenberg, M. Kazes, E. Shaviv and U. Banin, *Nano Lett.*, 2005, **5**, 1581–1586.
29 D. K. Sharma, S. Hirata, V. Biju and M. Vacha, *ACS Nano*, 2019, **13**, 624–632.
30 B. Lv, T. Zhu, Y. Tang, Y. Lv, C. Zhang, X. Wang, D. Shu and M. Xiao, *Phys. Rev. Lett.*, 2021, **126**, 197403.
31 L. Carbone, C. Nobile, M. De Giorgi, F. D. Sala, G. Morello, P. Pompa, M. Hytch, E. Snoeck, A. Fiore, I. R. Franchini, M. Nadasan, A. F. Silvestre, L. Chiodo, S. Kudera, R. Cingolani, R. Krahne and L. Manna, *Nano Lett.*, 2007, **7**, 2942–2950.
32 O. Chen, J. Zhao, V. P. Chauhan, J. Cui, C. Wong, D. K. Harris, H. Wei, H.-S. Han, D. Fukumura, R. K. Jain and M. G. Bawendi, *Nat. Mater.*, 2013, **12**, 445–451.
33 F. Hu, H. Zhang, C. Sun, C. Yin, B. Lv, C. Zhang, W. W. Yu, X. Wang, Y. Zhang and M. Xiao, *ACS Nano*, 2015, **9**, 12410–12416.
34 S. Morozov, E. L. Pensa, A. H. Khan, A. Polovitsyn, E. Cortés, S. A. Maier, S. Vezzoli, I. Moreels and R. Sapienza, *Sci. Adv.*, 2020, **6**, eabb1821.
35 Y.-S. Park, W. K. Bae, J. M. Pietryga and V. I. Klimov, *ACS Nano*, 2014, **8**, 7288–7296.
36 N. Hiroshige, T. Ihara, M. Saruyama, T. Teranishi and Y. Kanemitsu, *J. Phys. Chem. Lett.*, 2017, **8**, 1961–1966.
37 D. A. B. Miller, D. S. Chemla, T. C. Damen, A. C. Gossard, W. Wiegmann, T. H. Wood and C. A. Burrus, *Phys. Rev. Lett.*, 1984, **53**, 2173–2176.
38 H. Gotoh, H. Kamada, H. Ando and J. Temmyo, *Appl. Phys. Lett.*, 2000, **76**, 867–869.
39 X. Peng, M. C. Schlamp, A. V. Kadavanich and A. P. Alivisatos, *J. Am. Chem. Soc.*, 1997, **119**, 7019–7029.
40 N. Q. Huong and J. L. Birman, *J. Chem. Phys.*, 1998, **108**, 1769–1772.
41 A. Piryatinski, S. A. Ivanov, S. Tretiak and V. I. Klimov, *Nano Lett.*, 2007, **7**, 108–115.
42 H. Htoon, A. V. Malko, D. Bussian, J. Vela, Y. Chen, J. A. Hollingsworth and V. I. Klimov, *Nano Lett.*, 2010, **10**, 2401–2407.
43 Q. Xu, X. Huang, Z. Hua, L. Hu, L. Du, H. Wu, C. Zhang, X. Wang and M. Xiao, *Appl. Phys. Lett.*, 2016, **108**, 093110.

44 Al. L. Efros, M. Rosen, M. Kuno, M. Nirmal, D. J. Norris and M. Bawendi, *Phys. Rev. B: Condens. Matter Mater. Phys*, 1996, **54**, 4843–4856.
45 S. Brovelli, R. D. Schaller, S. A. Crooker, F. García-Santamaría, Y. Chen, R. Viswanatha, J. A. Hollingsworth, H. Htoon and V. I. Klimov, *Nat. Commun.*, 2011, **2**, 280.
46 S. A. Crooker, T. Barrick, J. A. Hollingsworth and V. I. Klimov, *Appl. Phys. Lett.*, 2003, **82**, 2793–2795.
47 A. F. Van Driel, G. Allan, C. Delerue, P. Lodahl, W. L. Vos and D. Vanmaekelbergh, *Phys. Rev. Lett.*, 2005, **95**, 236804.
48 L. Biadala, Y. Louyer, Ph. Tamarat and B. Lounis, *Phys. Rev. Lett.*, 2009, **103**, 037404.
49 N. S. Makarov, S. Guo, O. Isaienko, W. Liu, I. Robel and V. I. Klimov, *Nano Lett.*, 2016, **16**, 2349–2362.
50 S. J. W. Vonk, B. A. J. Heemskerk, R. C. Keitel, S. O. M. Hinterding, J. J. Geuchies, A. J. Houtepen and F. T. Rabouw, *Nano Lett.*, 2021, **21**, 5760–5766.
51 G. Nair, J. Zhao and M. G. Bawendi, *Nano Lett.*, 2011, **11**, 1136–1140.